JACS
JOURNAL OF THE AMERICAN CHEMICAL SOCIETY
Article
Cite This: J. Am. Chem. Soc. 2019, 141, 16408−16415
pubs.acs.org/JACS

Reversible Polymerization-like Kinetics for Programmable Self-Assembly of DNA-Encoded Nanoparticles with Limited Valence

Mengxin Gu, Xiaodong Ma, Liangshun Zhang,* and Jiaping Lin*

Shanghai Key Laboratory of Advanced Polymeric Materials, Key Laboratory for Ultrafine Materials of Ministry of Education, School of Materials Science and Engineering, East China University of Science and Technology, Shanghai 200237, China

Supporting Information

ABSTRACT: A similarity between the polymerization reaction of molecules and the self-assembly of nanoparticles provides a unique way to reliably predict structural characteristics of nanoparticle ensembles. However, the quantitative elucidation of programmable self-assembly kinetics of DNA-encoded nanoparticles is still challenging due to the existence of hybridization and dehybridization of DNA strands. Herein, a joint theoretical−computational method is developed to explicate the mechanism and kinetics of programmable self-assembly of limited-valence nanoparticles with surface encoding of complementary DNA strands. It is revealed that the DNA-encoded nanoparticles are programmed to form a diverse range of self-assembled superstructures with complex architecture, such as linear chains, sols, and gels of nanoparticles. It is theoretically demonstrated that the programmable self-assembly of DNA-encoded nanoparticles with limited valence generally obeys the kinetics and statistics of reversible step-growth polymerization originally proposed in polymer science. Furthermore, the theoretical−computational method is applied to capture the programmable self-assembly behavior of bivalent DNA−protein conjugates. The obtained results not only provide fundamental insights into the programmable self-assembly of DNA-encoded nanoparticles but also offer design rules for the DNA-programmed superstructures with elaborate architecture.

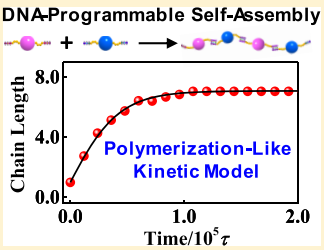

INTRODUCTION

Nanoparticles with surface encoding of DNA strands are widely regarded as "programmable atom-equivalents": Like atoms, the uniformly DNA-encoded nanoparticles (abbreviated as DNA-NPs) are directed to self-assemble into periodically crystalline structures; unlike atoms, the nanoparticles encoded by various DNA strands carry diversity and information that can be utilized to "program" a number of superlattice crystals through Watson−Crick base-pairing rules.[1−9] With the advances of nanotechnology, researchers have recently realized a novel system of nonuniform DNA-NPs with limited valence,[10−20] which have highly addressable and programmable surfaces. In comparison with the uniform system, such nanoparticles have the capability to control both the binding directionality and specificity, allowing for the programmable access to self-assemblies with unexpected complexity and diversity. For instance, multivalent nanoparticles regioselectively functionalized with DNA strands are programmed to self-assemble into sophisticated superstructures such as discrete dimers and necklaces,[12,16−20] which are common in the molecular system but rare in the system of uniform DNA-NPs. More recently, well-defined surfaces of proteins have provided an alternative possibility to construct bivalent DNA-NPs,[21−23] enabling the realization of one-dimensional chain-like superstructures. However, despite a significant step toward the addressable surfaces and many unique phenomena of self-assemblies, the universal principles (e.g., mechanism and kinetics) determining the collective self-assembly behavior of DNA-NPs remain unclear. A promising method to quantitatively predict the programmable self-assembly is to draw inspiration from the conceptual frameworks in atomic and molecular systems, such as reaction rate equations and detailed-balance principles.

Polymerization reaction, in which many reactive monomers are brought together and then form macromolecules,[24] bears strong similarities to the self-assembly behavior of anisotropic nanoparticles, such as self-repeating features of building units and topological characteristics of ensembles. Based on these similarities, an extension of molecular concepts to the self-assembly of anisotropic nanoparticles enables quantitative predictions of structural characteristics of nanoparticle ensembles.[25−38] A representative example is the self-assembly of patchy nanoparticles into supracolloidal polymers, whose growth can be described by the polymerization-like kinetics.[35−38] Although these investigations provide innovative proofs-of-concept, it is still challenging to quantitatively elucidate the programmable self-assembly kinetics of DNA-NPs with limited valence, due to the reversible and dynamic features of physical, noncovalent "bonds" originating from the hybridization and dehybridization of DNA strands.

To address these challenges, we integrate computer simulations and theoretical analyses to shed light on the programmable self-assembly behavior of DNA-NPs with limited valence. Specifically, the coarse-grained molecular dynamics is used to yield new insights into the mechanism

Received: July 24, 2019
Published: September 25, 2019

DOI: 10.1021/jacs.9b07919
J. Am. Chem. Soc. 2019, 141, 16408−16415

and kinetics of programmable self-assembly of DNA-NPs with various valences, as it was successfully applied to explicate the formation of superlattice crystals of nanoparticles.[39−43] The simulation outcomes are in good accordance with the theoretical predictions of the reversible step-growth polymerization model. Moreover, the joint theoretical−computational method allows us to reproduce the self-assembled superstructures of DNA−protein conjugates and further comprehend their self-assembly kinetics, which is currently difficult to achieve in experiments. This study will enable the precise construction of nanoparticle ensembles with controlled size and complex architecture, greatly broadening the scope and functionality of DNA-based materials.

RESULTS AND DISCUSSION

The generic coarse-grained model developed by Travesset's group is extended to probe important issues of programmable self-assembly of DNA-NPs with limited valence.[44−46] The system consists of a binary mixture of N_V V- and N_W W-type nanoparticles respectively dressed by f_V and f_W DNA strands. As a typical example, Figure 1a illustrates bivalent V- and W-type nanoparticles respectively dressed by two complementary DNA strands at their opposite poles. The coarse-grained simulations are performed under the canonical ensemble using the Nosé−Hoover thermostat,[47,48] where the diameter σ and mass m of beads as well as the potential strength ε are set as basic units. The reduced temperature is denoted by $T^* = k_BT/\varepsilon$, and the simulation time is measured in units of τ. The initial concentration of DNA strands attached onto the V-type nanoparticles is defined as $c_0 = N_V f_V/L^3$, where L is the size of simulation boxes. Unless otherwise stated, the total numbers of sequence-specific DNA strands attached onto the V- and W-type nanoparticles are equal. The detailed descriptions of the model and simulation protocol can be seen in Part 1 of the Supporting Information (SI).

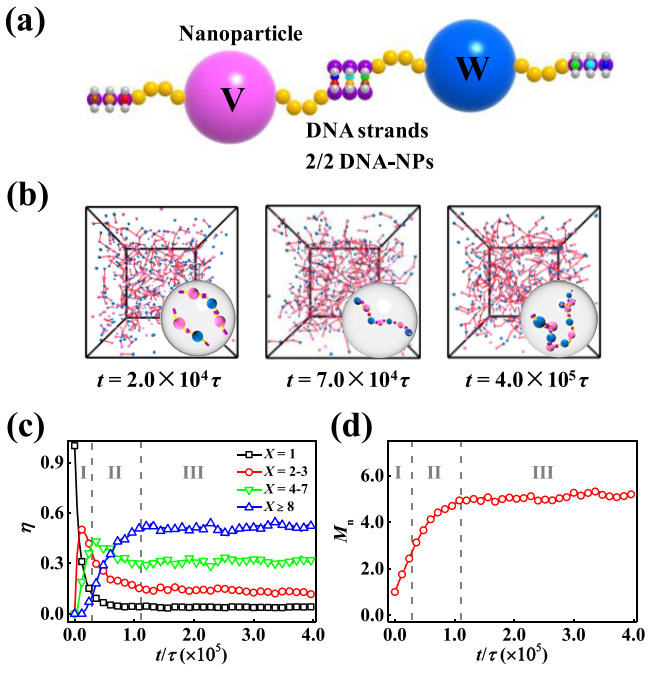

Figure 1. (a) Schematic representation of programmable self-assembly for the binary mixture of bivalent V- and W-type nanoparticles. (b) Set of snapshots of programmable self-assembled superstructures. Red lines represent the connections between the V- and W-type nanoparticles. Insets illustrate the representative configurations of superstructures. (c) Temporal evolution of weight fraction η of chain-like superstructures consisting of X nanoparticles. (d) Temporal evolution of number-average length M_n of nanoparticle chains. Vertical dashed lines indicate approximate boundaries between different stages of programmable self-assembly. The error bars are not shown for clarity. The reduced temperature and the initial concentration are fixed at $T^* = 0.90$ and $c_0 = 1.3 \times 10^{-4}\ \sigma^{-3}$, respectively.

Mechanism of Programmable Self-Assembly of DNA-NPs. Figure 1b displays a set of snapshots of DNA-programmed superstructures for the binary mixture of bivalent nanoparticles (designated as 2/2 DNA-NPs).[49] Initially, free nanoparticles acting as building units are mutually connected to form dimers and trimers, driven by the DNA hybridization between the complementary bases of sticky ends. Subsequently, the existence of free sticky ends at terminations enables their further growth to yield nanoparticle oligomers. Finally, the binary mixture of nanoparticles self-assembles into long polymer-like chains with an alternating arrangement of V- and W-type nanoparticles. Our coarse-grained simulations well reproduce the experimental observations of self-assembly of DNA-NPs.[12,16,19] However, a fundamental exploration of the mechanism and kinetics of programmable self-assembly is still pending due to the limitations of experimental techniques.

To quantitatively describe the self-assembly behavior, DNA-programmed superstructures are distinguished by a general distance criterion, and their length corresponds to the number of nanoparticles. For clarity, the superstructures are roughly divided into four subsets according to their length X, where $X = 1$ (monomers of nanoparticles), $X = 2$, 3 (dimers and trimers), $X = 4-7$ (oligomers), and $X \geq 8$ (polymers). Populations of different subsets of superstructures are measured by their weight fraction η defined as $\eta_{X=a\rightarrow b} = \sum_{X=a}^{b} X n_X/N$, where n_X denotes the number of superstructures containing X nanoparticles and N represents the total number of nanoparticles. The number-average length M_n of chain-like superstructures is represented by $M_n = N/\sum_X n_X$.

Figure 1c and d display the weight fraction η of different subsets and the number-average length M_n of chain-like superstructures in terms of the time, respectively. On the basis of the temporal evolution of η, we divide the self-assembly process into three stages. In stage I, the consumption of free nanoparticles accounts for the formation of short chains including dimers, trimers, and oligomers. The length M_n of nanoparticle chains shows a linear dependence with the time. In stage II, the fraction of short chains shows a decrease, while the fraction of long chains increases rapidly, suggesting that the elongation of nanoparticle chains originates from the coupling between existing short chains instead of the sequential addition of free nanoparticles (i.e., a salient feature of step-growth polymerization). Consequently, the growth rate of nanoparticle chains slows down. In stage III, the nanoparticle chains with various lengths coexist in the system and their respective fraction remains constant. As a result, the number-average length of nanoparticle chains reaches a plateau.

To further probe the growth pathway of nanoparticle chains over three stages, we select individual chains and trace the chain length X, which is plotted in Figure 2a. The curves exhibit alternating jump-ups and jump-downs, suggesting that the superstructures are elongated/broken through the hybridization of DNA strands and the dehybridization of DNA duplexes. To characterize the elongation and breaking of

DOI: 10.1021/jacs.9b07919
J. Am. Chem. Soc. 2019, 141, 16408−16415

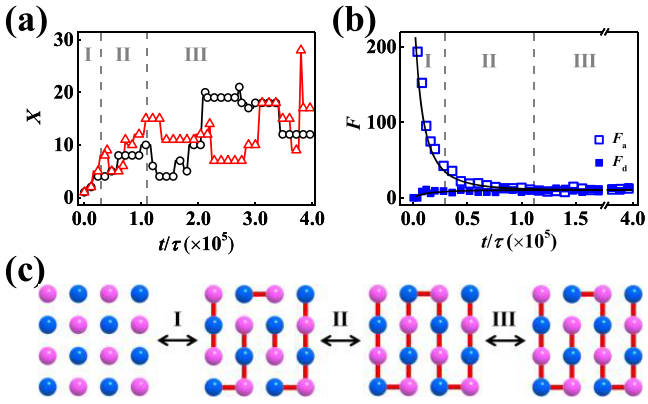

Figure 2. (a) Length X of representative nanoparticle chains in terms of the time t. (b) Occurrence frequencies F_a and F_d of assembly and disassembly events of nanoparticle chains in terms of the time t. (c) Schematic illustration of the self-assembly pathway of DNA-NPs via hybridization/dehybridization of DNA strands. The V- and W-type DNA-NPs are represented by the spheres with distinct colors, and their connections are shown by the red-colored lines.

nanoparticle chains, we analyze the occurrence frequencies (F_a and F_d) of assembly and disassembly of nanoparticle chains in the time interval ΔI, e.g., $\Delta I = 4000.0\tau$ (Figure 2b). In stage I, due to the existence of large amounts of free DNA sticky ends, the occurrence frequency of nanoparticle assembly far exceeds that of disassembly, which promotes the elongation of nanoparticle chains. In stage II, the continuous consumption of residual DNA sticky ends leads to a reduction in the assembly frequency. In stage III, the occurrence frequencies of assembly and disassembly of nanoparticle chains are very close, indicating that the formed chains of nanoparticles are dynamic, breaking and recoupling.

Figure 2c outlines all the programmable self-assembly pathways of divalent nanoparticles functionalized with complementary DNA strands. The hybridization of DNA strands and the dehybridization of DNA duplexes promote the dynamic interconversion between self-assembled superstructures through three distinct processes: addition of free nanoparticles into short chains, coupling of short chains into long ones, and breaking of long chains into short ones. Namely, the bivalent DNA-NPs behave as bifunctional molecules. The V- and W-type DNA-NPs in the chain-like superstructures correspond to the repeat units of molecular polymers, and the complementary base pairs of sticky ends act as physical, noncovalent "bonds". The growth of chain-like superstructures undergoes the nanoparticle monomer ↔ oligomer ↔ polymer pathway. Therefore, these phenomena observed from Figures 1 and 2 manifest the fact that the programmable self-assembly of DNA-NPs into chain-like superstructures is markedly analogous to the reversible step-growth polymerization of molecules instead of the living polymerization, which is further demonstrated by the distribution of the number fraction of nanoparticle chains (Figure S3.1 of the SI).

Kinetics of Programmable Self-Assembly of DNA-NPs. Below, we generalize Flory's model of molecular polymerization in polymer science to conceptualize and quantify the self-assembly kinetics of DNA-NPs.[24,50] The formation of superstructures with x and y repeat units can be cast by a series of parallel "chemical reactions"

$$\text{V-W}_x + \text{V-W}_y \underset{k_d}{\overset{k_a}{\rightleftharpoons}} \text{V-W}_{x+y+1}$$

where k_a and k_d respectively represent the rate constants of assembly and disassembly of superstructures. The wavy lines denote the possible V- or W-type nanoparticles connecting with repeat units. The hybridization extent of DNA strands attached onto the V-type nanoparticles is represented by $p = (c_0 - c)/c_0$, and its equilibrium value is designated as p_e, where c is the concentration of residual DNA strands. The apparent equilibrium constant is given by $K/\sigma^3 \equiv k_a/k_d = p_e/c_0(1 - p_e)^2$. On the basis of the relationship $M_n = 1/(1 - p)$ for the binary mixture of 2/2 DNA-NPs, the analytical expression of number-average length M_n of nanoparticle chains is written as

$$M_n = 1 + \frac{p_e(e^{k_a c_0(1-p_e^2)t/p_e} - 1)}{(1 - p_e)(e^{k_a c_0(1-p_e^2)t/p_e} + p_e)} \quad (1)$$

Full details on the generalization of the theoretical model can be found in Part 2 of the SI.

Similar to the reaction kinetics of molecules, the self-assembly kinetics of DNA-NPs described by eq 1 can be finely tuned by modulating the initial concentration c_0 of DNA strands. Figure 3a shows the number-average length M_n of

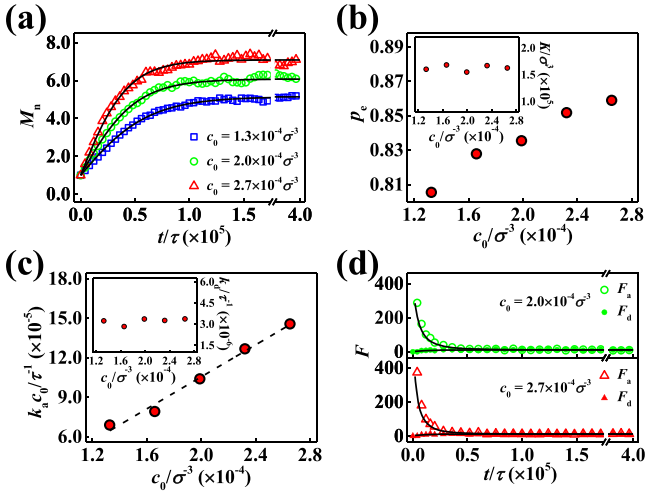

Figure 3. Effect of initial concentration c_0 on programmable self-assembly of bivalent DNA-NPs. (a) Temporal evolution of number-average length M_n of nanoparticle chains under various initial concentrations c_0. The solid lines denote the fitting curves of the theoretical model. (b) Equilibrium hybridization extent p_e and apparent equilibrium constant K (inset) in terms of the initial concentration c_0. (c) Combined assembly rate coefficient $k_a c_0$ and disassembly rate constant k_d (inset) in terms of the initial concentration c_0. The dashed line shows the linear relationship between $k_a c_0$ and c_0. (d) Occurrence frequencies F_a and F_d of assembly and disassembly events of nanoparticle chains in terms of the time t. The reduced temperature is set as $T^* = 0.90$.

nanoparticle chains in terms of the assembly time under various initial concentrations c_0. High initial concentration c_0 accelerates the growth of nanoparticle chains and results in a larger value of M_n at a given time. The simulation data are well captured by our proposed model based on the kinetics of reversible step-growth polymerization. Through fitting the simulation data to eq 1, the obtained equilibrium value p_e of hybridization extent and the combined value of $k_a c_0$ are used to deduce the apparent equilibrium constant K and the

DOI: 10.1021/jacs.9b07919
J. Am. Chem. Soc. 2019, 141, 16408−16415

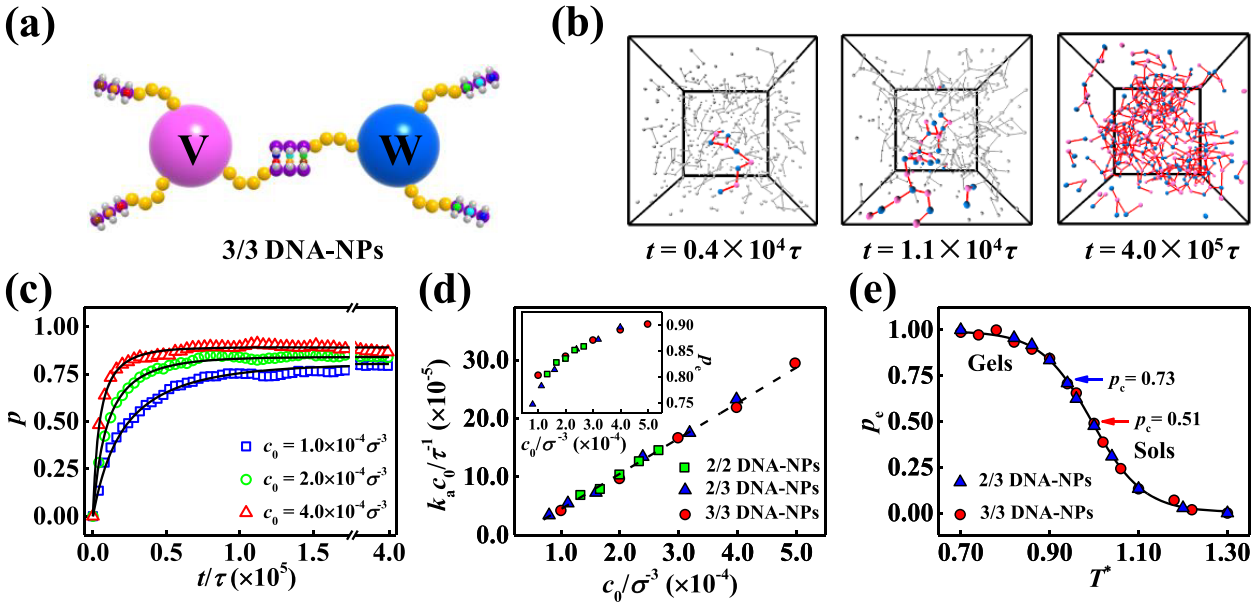

Figure 4. (a) Schematic representation of programmable self-assembly for the binary mixture of trivalent V- and W-type nanoparticles. (b) Set of snapshots of self-assembled superstructures. The largest superstructure is highlighted. The reduced temperature is set as $T^* = 0.90$, and the initial concentration $c_0 = 2.0 \times 10^{-4}\ \sigma^{-3}$. (c) Temporal evolution of hybridization extent p of DNA strands under various initial concentrations c_0. (d) Combined assembly rate coefficient $k_a c_0$ and equilibrium hybridization extent p_e (inset) as a function of the initial concentration c_0 for the programmable self-assembly of binary mixtures of 2/2, 2/3, and 3/3 DNA-NPs. The dashed line shows the linear relationship between $k_a c_0$ and c_0. The reduced temperature is set as $T^* = 0.90$. (e) Equilibrium hybridization extent p_e as a function of the reduced temperature T^* for the programmable self-assembly of binary mixtures of 2/3 and 3/3 DNA-NPs. The arrows highlight the critical values p_c of hybridization extent for the sol-to-gel transition. The initial concentration is set as $c_0 = 2.0 \times 10^{-4}\ \sigma^{-3}$.

disassembly rate constant k_d (Figure 3b and c). An increase in the initial concentration c_0 results in larger values of p_e and $k_a c_0$. However, the apparent equilibrium constant K and the disassembly rate constant k_d are weakly dependent upon the initial concentration c_0. It should be mentioned that the dashed line in Figure 3c represents the fitting curve of combined value $k_a c_0$ versus c_0, which yields the rate constant $k_a = 0.61\sigma^3\tau^{-1}$ of programmable self-assembly of bivalent DNA-NPs.

Figures 2b and 3d show the effect of initial concentration c_0 on the occurrence frequencies (F_a and F_d) of assembly and disassembly of nanoparticle chains. In the case of a high initial concentration c_0, F_a has a large value in the initial stage. However, F_a and F_d reach a comparable plateau in the late stage, whose value is weakly dependent upon the initial concentration c_0. The solid lines in Figures 2b and 3d display the theoretically predicted values of F_a and F_d from the reversible step-growth polymerization model (the case of $r = 1.0$ in eq S-2.1 of the SI), i.e., $F_a = k_a c_0^2(1-p)^2 L^3 \Delta I$ and $F_d = k_d c_0 p L^3 \Delta I$. The good agreement between the theoretical predictions and the simulation outcomes further supports the findings that our proposed model of reversible step-growth polymerization has the capability to describe the programmable self-assembly kinetics of DNA-NPs.

Because of the incorporation of molecular information on DNA strands into the mesoscopic system, the self-assembly kinetics of DNA-NPs is also affected by the physiochemical properties of DNA strands (e.g., reduced temperature T^*, linker length n_l, and spacer length n_s of DNA strands as well as initial ingredient r), which are shown in Figures S3.2−S3.5 of the SI. It is worthwhile pointing out that the initial ingredient of the binary mixture markedly affects the growth of chain-like superstructures, which can be utilized to tune the length of nanoparticle chains. In addition, the thermodynamics of self-assembly of DNA-NPs such as free energy ΔG and activation energy E_a can be extracted from the relationship between the reduced temperature and the apparent equilibrium constant K as well as the disassembly rate constant k_d (Figure S3.6 of the SI).

In comparison with the polymerization of molecules, the polymerization-like kinetics of bivalent DNA-NPs possesses inherent characteristics. Specifically, the rate constant $k_a = 0.61\sigma^3\tau^{-1} \approx 7.34 \times 10^{10}$ L·mol^{-1}·s^{-1} is notably larger than that of the molecular system (about 10^{-3}−10^{-5} L·mol^{-1}·s^{-1}).[50] More importantly, the programmable self-assembly kinetics of DNA-NPs can be efficiently tuned by the molecular design of DNA strands (e.g., linker length of DNA strands), which provides new opportunities for constructing the hierarchical superstructures.

Generalization of Polymerization-like Kinetics. Considering the fundamental resemblance between the programmable self-assembly of DNA-NPs and the polymerization of molecular monomers described above, the design rules of building units used to construct nonlinear polymers are generalized to enable the realization of self-assembled superstructures with complex architecture.[51−53] Similar to the experimentally realized system of nonlinear polymers, trivalent nanoparticles in the coarse-grained simulations are functionalized with three DNA strands, which are equally spaced on the equator. Below, two types of programmable self-assembly system of DNA-NPs are considered: one is the binary mixture of trivalent V- and W-type nanoparticles (coded as 3/3 DNA-NPs, Figure 4a), and the other is the binary mixture of bivalent V-type and trivalent W-type DNA-NPs (2/3 DNA-NPs, Figure S4.1a of the SI). Herein, the total numbers of DNA strands attached onto the V- and W-type nanoparticles are equal. The hybridization of complementary DNA strands drives the

DOI: 10.1021/jacs.9b07919
J. Am. Chem. Soc. 2019, 141, 16408−16415

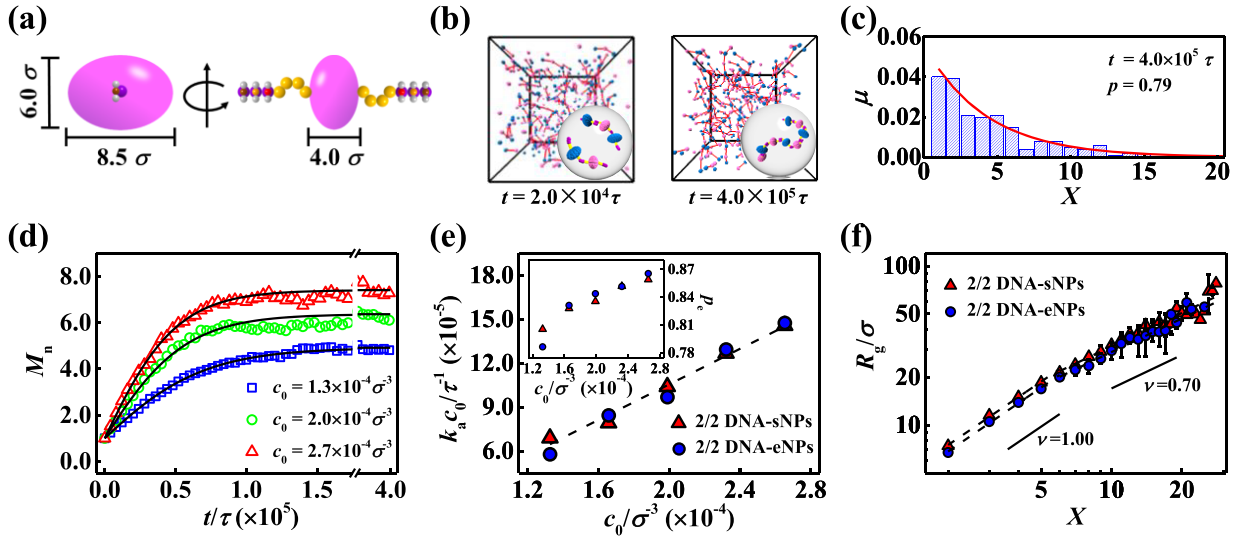

Figure 5. (a) Coarse-grained model of ellipsoidal V-type DNA-NPs with dimensions $8.5\sigma \times 6.0\sigma \times 4.0\sigma$. (b) Self-assembled superstructures of a binary mixture of ellipsoidal V- and W-type DNA-NPs. (c) Number fraction μ of nanoparticle chains as a function of the chain length X. (d) Temporal evolution of number-average length M_n of nanoparticle chains. In panels (c) and (d), the solid lines represent the fitting curves of the theoretical model. (e) Combined assembly rate coefficient $k_a c_0$ and equilibrium hybridization extent p_e (inset) as a function of the initial concentration c_0 for the spherical and ellipsoidal nanoparticles (coded as 2/2 DNA-sNPs and DNA-eNPs, respectively). (f) Double-logarithmic plot of gyration radius R_g of nanoparticle chains versus the chain length X. Solid lines represent the best-fit scaling law (i.e., $R_g \sim X^{\nu}$) in the range of short and long chains of nanoparticles. The reduced temperature is set as $T^* = 0.90$, and the initial concentration $c_0 = 1.3 \times 10^{-4}\ \sigma^{-3}$.

trivalent nanoparticles as branching points to self-assemble into the finite-size clusters (i.e., nanoparticle sols) with branched architecture, and the small clusters are coalesced to eventually form network-like superstructures (i.e., nanoparticle gels) spanning the entire box of simulations, which are depicted in Figures 4b and S4.1b of the SI. Correspondingly, the self-assembly mechanism of multivalent DNA-NPs is schematically illustrated in Figure S4.2 of the SI. It should be mentioned that such novel superstructures with complex architecture cannot be produced by the programmable self-assembly of a binary mixture of 2/2 DNA-NPs.

For the programmable self-assembly kinetics of multivalent DNA-NPs, it is straightforward to evaluate the time-dependent hybridization extent p of DNA strands (Figures 4c and S4.1c of the SI).[54−57] During the coarse-grained simulations, the value of p rapidly increases in the initial stage and gradually reaches its equilibrium value p_e in the late stage. Because the programmable self-assembly of multivalent DNA-NPs shares conceptual similarities with the reversible step-growth polymerization of multifunctional molecules, the analytical expression of hybridization extent p can be derived from our proposed model of step-growth polymerization (Part 2 of the SI). A fitting of simulation data to eq S-2.2 of the SI yields the combined value $k_a c_0$ of assembly rate constant and the equilibrium value p_e of hybridization extent (Figure 4d). Notably, the data of $k_a c_0$ versus c_0 for different systems of binary mixtures collapse on a master curve, which yields the rate constant $k_a = 0.61\sigma^3\tau^{-1}$ of programmable self-assembly of DNA-NPs with various valences. It should be mentioned that the influence of reduced temperature on the self-assembly kinetics of multivalent DNA-NPs is also captured by our proposed model (Figure S4.3 of the SI). Unlike the earlier works on the single-component system of multivalent DNA-NPs,[56−59] a salient feature of the binary system of DNA-NPs is that the self-assembly kinetics and self-assembled superstructures of DNA-NPs can be finely tuned by changing the initial ingredient (Figure S4.4 of the SI). These observations verify the fact that the conceptual framework of polymerization-like kinetics of bivalent DNA-NPs can be generalized to describe the programmable self-assembly behavior of multivalent DNA-NPs.

The presence of trivalent nanoparticles in the binary mixture introduces one important phenomenon (i.e., a sol-to-gel or percolation transition from finite to infinite clusters of nanoparticles, as shown in Figures 4b and S4.1b of the SI), which is missing in the programmable self-assembly of bivalent DNA-NPs. The Flory−Stockmayer theory on the cross-linking and gelation of multifunctional molecules is able to provide mean-field predictions for the distribution of cluster size (Figure S4.5 of the SI) and the location of sol-to-gel transition (Figure S4.6 of the SI).[24,60] For the binary mixtures of 3/3 and 2/3 DNA-NPs, the critical values p_c of hybridization extent for the sol-to-gel transition are $p_c = 0.51$ and 0.73, respectively. The critical values can be used to identify the self-assembled superstructures of DNA-NPs, which are tightly correlated with the reduced temperature and the initial concentration. As a representative example, Figure 4e depicts the temperature dependence of equilibrium hybridization extent p_e for the binary mixtures of 2/3 and 3/3 DNA-NPs. As the reduced temperature is increased, the self-assembled superstructures of trivalent DNA-NPs switch from the gels (i.e., infinite spanning clusters under the condition of $p_e \geq p_c$) to sols (finite clusters in the case of $p_e < p_c$) and finally to monomeric nanoparticles. Thus, our findings suggest that the rational design and use of DNA-NPs with limited valence make it possible to generate thermoreversible gels, which can be used to realize soft materials with promising horizons for biomedical applications. It should be mentioned that above a critical value of the valence of DNA-NPs the crystalline phase of DNA-NPs is more favorable than the gel-like superstructures.[61,62]

Experimental Discussion. So far, there are no relevant studies on the programmable self-assembly of limited-valence

DOI: 10.1021/jacs.9b07919
J. Am. Chem. Soc. 2019, 141, 16408−16415

DNA-NPs with a spherical shape. Thus, the comparison between the experimental findings and the theoretical predictions remains difficult to realize. However, there are still some experimental observations with respect to the self-assembled superstructures of nonspherical DNA-NPs with limited valence.[12,16,22,23] For instance, Mirkin's group have recently synthesized bivalent proteins functionalized with DNA strands at the opposing ends of their surfaces,[22,23] which allow one to engineer directional interactions. It was demonstrated that such bivalent DNA−protein conjugates are programmed to self-assemble into chain-like superstructures, which are reasonably reproduced by the coarse-grained simulations of DNA-NPs with a spherical shape (coded as DNA-sNPs below, Figure 1).

To thoroughly elucidate the programmable self-assembly of bivalent DNA−protein conjugates, we construct the coarse-grained model by considering the shape of proteins. The proteins are modeled by ellipsoidal rigid bodies (coded as DNA-eNPs, Figure 5a),[21] which are dressed by two DNA strands. As illustrated in Figure 5b, the DNA-eNPs are programmed to self-assemble into chain-like superstructures. Despite the use of the coarse-grained model of bivalent DNA−protein conjugates, the theoretical predictions in accordance with the experimental observations unequivocally confirm the role of bivalent DNA-NPs for the chain-like superstructures.

As illustrated in Figure 5c, the number fraction $\mu \equiv n_X/N$ of nanoparticle chains in terms of the chain length X can be fitted by the Flory−Schulz distribution, i.e., $\mu = p^{X-1}(1 - p)^2$.[24] It should be noted that the distribution of number fraction in the experimental works shows a peak.[22,23] One of the reasons for the deviation between the experimental and our works comes from the different self-assembly strategies of DNA−protein conjugates (Figure S5.1 of the SI).

More importantly, the coarse-grained model can be applied to probe the self-assembly kinetics of DNA−protein conjugates and the conformational statistics of chain-like superstructures, which are currently challenging to evaluate in experiments. Figure 5d displays the number-average length M_n of self-assembled superstructures in terms of time. The self-assembly kinetics of DNA−protein conjugates can be captured by our proposed model of reversible step-growth polymerization. The combined assembly rate coefficient $k_a c_0$ and the equilibrium hybridization extent p_e are close to those of spherical nanoparticles (Figure 5e).

Inspired by the scaling theory of molecular polymers,[19,24,63] we further analyze the gyration radius R_g of chain-like superstructures containing X nanoparticles, defined as $R_g^2 \equiv \langle \sum_{j=1}^{X} (\mathbf{R}_j - \mathbf{R}_c)^2 \rangle / X$, where $\mathbf{R}_j$ is the coordinates of jth nanoparticle and $\mathbf{R}_c$ is the position of the center-of-mass of the self-assembled superstructure. Figure 5f (also Figure S3.7 of the SI) shows the relationship between the gyration radius and the chain length for the DNA-sNPs and DNA-eNPs. In both cases, the radius of gyration in terms of the chain length obeys the scaling law, i.e., $R_g \sim X^{\nu}$, where the scaling exponent ν is varied over the range of chain length. In the case of short nanoparticle chains, the size of self-assembled superstructures increases as a function of $X^{1.00}$, which is the scaling law of rod-like polymers. As nanoparticle chains become long, most of the data points follow the $X^{0.70}$ relationship, which has a slight deviation from the good-solvent scaling law $X^{0.60}$ of linear polymer chains. It should be pointed out that the dependence of gyration radius of branched clusters of DNA-NPs on their size is weaker than that of chain-like superstructures (Figure S4.7 of the SI).

As illustrated above, the reversible polymerization-like mechanism and kinetics for the programmable self-assembly of bivalent DNA-NPs are valid for the system of DNA−protein conjugates. Thus, the results together with the findings of Part 3 of the SI provide significant information to kinetically control the size and dispersity of chain-like superstructures (Figure S5.1 of the SI). Furthermore, our findings of multivalent DNA-NPs will facilitate the design of new, complex superstructures of DNA−protein conjugates by mimicking a large library of molecular polymers, e.g., hyperbranches and networks (Figure S5.2 of the SI), whose internal architecture is regulated by the molecular design of DNA strands (Figure S4.8 of the SI).

Finally, it is worthwhile pointing out that the model of step-growth polymerization is also able to describe the self-assembly kinetics of patchy nanoparticles. However, there are some differences between the polymerization-like kinetics of patchy nanoparticles and that of DNA-NPs. Specifically, the self-assembly kinetics of patchy particles is generally modeled by the irreversible step-growth polymerization due to the formation of permanent "bonds".[25,32−34] By contrast, the programmable self-assembly of DNA-NPs resembles the reversible step-growth polymerization of molecules, owing to the hybridization and dehybridization of DNA strands. Another significant characteristic of the DNA-NP system is the constant rate coefficient of self-assembly. However, the self-assembly of patchy nanoparticles satisfies the diffusion-controlled kinetics with a variable rate coefficient,[37,38] due to the conformational characteristics of self-assembled superstructures. These differences mentioned above pinpoint the significance of design rules of nanosized building units, which have a tight relationship with their self-assembly kinetics.

CONCLUSIONS

In summary, the joint theoretical−computational method is proposed to investigate the programmable self-assembly of DNA-encoded nanoparticles with limited valence. Driven by the hybridization of DNA strands, the binary mixture of bivalent nanoparticles is programmed to self-assemble into the chain-like superstructures. The incorporation of multivalent nanoparticles results in the achievement of self-assembled superstructures with complex architecture, such as sols and gels of nanoparticles. It is demonstrated that the kinetics of programmable self-assembly is conceptually identical and quantitatively comparable to that of reversible step-growth polymerization. Furthermore, the simulations and theoretical analyses can reproduce the experimental observations of programmable self-assembly of bivalent DNA−protein conjugates and capture their self-assembly kinetics. Our findings bear wide implications for quantitatively predicting the self-assembled superstructures and self-assembly kinetics of DNA-encoded nanoparticles with limited valence, which will considerably facilitate the experimental realization of hierarchical self-assemblies with controlled size and complex architecture.

ASSOCIATED CONTENT

Supporting Information

The Supporting Information is available free of charge on the ACS Publications website at DOI: 10.1021/jacs.9b07919.

DOI: 10.1021/jacs.9b07919
J. Am. Chem. Soc. 2019, 141, 16408−16415

Details of computational and theoretical models; additional results and corresponding figures (PDF)

AUTHOR INFORMATION

Corresponding Authors

*zhangls@ecust.edu.cn

*jlin@ecust.edu.cn

ORCID

Liangshun Zhang: 0000-0002-0182-7486

Jiaping Lin: 0000-0001-9633-4483

Notes

The authors declare no competing financial interest.

ACKNOWLEDGMENTS

This work was supported by the National Natural Science Foundation of China (21574040, 21873029, and 51833003). We are grateful to Prof. R. Wang of NJU and Prof. H. Liang of USTC for their valuable comments. We sincerely thank the anonymous reviewers for their helpful suggestions, which resulted in substantial improvements of this work.

REFERENCES

(1) Mirkin, C. A.; Letsinger, R. L.; Mucic, R. C.; Storhoff, J. J. A DNA-Based Method for Rationally Assembling Nanoparticles into Macroscopic Materials. *Nature* **1996**, *382*, 607−609.

(2) Alivisatos, A. P.; Johnsson, K. P.; Peng, X.; Wilson, T. E.; Loweth, C. J.; Bruchez, M. P., Jr; Schultz, P. G. Organization of "Nanocrystal Molecules" Using DNA. *Nature* **1996**, *382*, 609−611.

(3) Nykypanchuk, D.; Maye, M. M.; van der Lelie, D.; Gang, O. DNA-Guided Crystallization of Colloidal Nanoparticles. *Nature* **2008**, *451*, 549−552.

(4) Park, S. Y.; Lytton-Jean, A. K. R.; Lee, B.; Weigand, S.; Schatz, G. C.; Mirkin, C. A. DNA-Programmable Nanoparticle Crystallization. *Nature* **2008**, *451*, 553−556.

(5) Macfarlane, R. J.; Lee, B.; Jones, M. R.; Harris, N.; Schatz, G. C.; Mirkin, C. A. Nanoparticle Superlattice Engineering with DNA. *Science* **2011**, *334*, 204−208.

(6) Macfarlane, R. J.; O'Brien, M. N.; Petrosko, S. H.; Mirkin, C. A. Nucleic Acid-Modified Nanostructures as Programmable Atom Equivalents: Forging a New "Table of Elements". *Angew. Chem., Int. Ed.* **2013**, *52*, 5688−5698.

(7) Auyeung, E.; Li, T. I. N. G.; Senesi, A. J.; Schmucker, A. L.; Pals, B. C.; Olverade la Cruz, M.; Mirkin, C. A. DNA-Mediated Nanoparticle Crystallization into Wulff Polyhedra. *Nature* **2014**, *505*, 73−77.

(8) Rogers, W. B.; Manoharan, V. N. Programming Colloidal Phase Transitions with DNA Strand Displacement. *Science* **2015**, *347*, 639−642.

(9) Rogers, W. B.; Shih, W. M.; Manoharan, V. N. Using DNA to Program the Self-Assembly of Colloidal Nanoparticles and Microparticles. *Nat. Rev. Mater.* **2016**, *1*, 16008.

(10) Maye, M. M.; Nykypanchuk, D.; Cuisinier, M.; van der Lelie, D.; Gang, O. Stepwise Surface Encoding for High-Throughput Assembly of Nanoclusters. *Nat. Mater.* **2009**, *8*, 388−391.

(11) Jones, M. R.; Macfarlane, R. J.; Lee, B.; Zhang, J.; Young, K. L.; Senesi, A. J.; Mirkin, C. A. DNA-Nanoparticle Superlattices Formed from Anisotropic Building Blocks. *Nat. Mater.* **2010**, *9*, 913−917.

(12) Wang, Y.; Wang, Y.; Breed, D. R.; Manoharan, V. N.; Feng, L.; Hollingsworth, A. D.; Weck, M.; Pine, D. J. Colloids with Valence and Specific Directional Bonding. *Nature* **2012**, *491*, 51−55.

(13) Feng, L.; Dreyfus, R.; Sha, R.; Seeman, N. C.; Chaikin, P. M. DNA Patchy Particles. *Adv. Mater.* **2013**, *25*, 2779−2783.

(14) O'Brien, M. N.; Jones, M. R.; Lee, B.; Mirkin, C. A. Anisotropic Nanoparticle Complementarity in DNA-Mediated Co-Crystallization. *Nat. Mater.* **2015**, *14*, 833−839.

(15) Edwardson, T. G.; Lau, K. L.; Bousmail, D.; Serpell, C. J.; Sleiman, H. F. Transfer of Molecular Recognition Information from DNA Nanostructures to Gold Nanoparticles. *Nat. Chem.* **2016**, *8*, 162.

(16) Chen, G.; Gibson, K. J.; Liu, D.; Rees, H. C.; Lee, J.-H.; Xia, W.; Lin, R.; Xin, H. L.; Gang, O.; Weizmann, Y. Regioselective Surface Encoding of Nanoparticles for Programmable Self-Assembly. *Nat. Mater.* **2019**, *18*, 169−174.

(17) Zhang, Y.; McMullen, A.; Pontani, L.-L.; He, X.; Sha, R.; Seeman, N. C.; Brujic, J.; Chaikin, P. M. Sequential Self-Assembly of DNA Functionalized Droplets. *Nat. Commun.* **2017**, *8*, 21.

(18) Zhang, Y.; He, X.; Zhuo, R.; Sha, R.; Brujic, J.; Seeman, N. C.; Chaikin, P. M. Multivalent, Multiflavored Droplets by Design. *Proc. Natl. Acad. Sci. U. S. A.* **2018**, *115*, 9086−9091.

(19) McMullen, A.; Holmes-Cerfon, M.; Sciortino, F.; Grosberg, A. Y.; Brujic, J. Freely Jointed Polymers Made of Droplets. *Phys. Rev. Lett.* **2018**, *121*, 138002.

(20) Lin, Z.; Xiong, Y.; Xiang, S.; Gang, O. Controllable Covalent-Bound Nano-Architectures from DNA Frames. *J. Am. Chem. Soc.* **2019**, *141*, 6797−6801.

(21) McMillan, J. R.; Brodin, J. D.; Millan, J. A.; Lee, B.; Olvera de la Cruz, M.; Mirkin, C. A. Modulating Nanoparticle SuperlatticeStructure Using Proteins with Tunable Bond Distributions. *J. Am. Chem. Soc.* **2017**, *139*, 1754−1757.

(22) McMillan, J. R.; Mirkin, C. A. DNA-Functionalized, Bivalent Proteins. *J. Am. Chem. Soc.* **2018**, *140*, 6776−6779.

(23) McMillan, J. R.; Hayes, O. G.; Remis, J. P.; Mirkin, C. A. Programming Protein Polymerization with DNA. *J. Am. Chem. Soc.* **2018**, *140*, 15950−15956.

(24) Flory, P. J. *Principles of Polymer Chemistry*; Cornell University Press: Ithaca, NY, 1953.

(25) Liu, K.; Nie, Z.; Zhao, N.; Li, W.; Rubinstein, M.; Kumacheva, E. Step-Growth Polymerization of Inorganic Nanoparticles. *Science* **2010**, *329*, 197−200.

(26) Chen, Q.; Whitmer, J. K.; Jiang, S.; Bae, S. C.; Luijten, E.; Granick, S. Supracolloidal Reaction Kinetics of Janus Spheres. *Science* **2011**, *331*, 199−202.

(27) Klinkova, A.; Thérien-Aubin, H.; Choueiri, R. M.; Rubinstein, M.; Kumacheva, E. Colloidal Analogs of Molecular Chain Stoppers. *Proc. Natl. Acad. Sci. U. S. A.* **2013**, *110*, 18775−18779.

(28) Gröschel, A. H.; Walther, A.; Löbling, T. I.; Schacher, F. H.; Schmalz, H.; Müller, A. H. E. Guided Hierarchical Co-Assembly of Soft Patchy Nanoparticles. *Nature* **2013**, *503*, 247−251.

(29) Wang, J.; Xia, H.; Zhang, Y.; Lu, H.; Kamat, R.; Dobrynin, A. V.; Cheng, J.; Lin, Y. Nucleation-Controlled Polymerization of Nanoparticles into Supramolecular Structures. *J. Am. Chem. Soc.* **2013**, *135*, 11417−11420.

(30) Luo, B.; Smith, J. W.; Wu, Z.; Kim, J.; Ou, Z.; Chen, Q. Polymerization-Like Co-Assembly of Silver Nanoplates and Patchy Spheres. *ACS Nano* **2017**, *11*, 7626−7633.

(31) Kim, J.; Ou, Z.; Jones, M. R.; Song, X.; Chen, Q. Imaging the Polymerization of Multivalent Nanoparticles in Solution. *Nat. Commun.* **2017**, *8*, 761.

(32) Sciortino, F.; Bianchi, E.; Douglas, J. F.; Tartaglia, P. Self-Assembly of Patchy Particles into Polymer Chains: A Parameter-Free Comparison between Wertheim Theory and Monte Carlo Simulation. *J. Chem. Phys.* **2007**, *126*, 194903.

(33) Corezzi, S.; Michele, C. D.; Zaccarelli, E.; Fioretto, D.; Sciortino, F. A Molecular Dynamics Study of Chemical Gelation in a Patchy Particle Model. *Soft Matter* **2008**, *4*, 1173−1177.

(34) Tavares, J. M.; Teixeira, P. I. C.; da Gama, M. T. Criticality of Colloids with Distinct Interaction Patches: The Limits of Linear Chains, HyperbranchedPolymers, and Dimers. *Phys. Rev. E* **2009**, *80*, 021506.

(35) Zhuang, Z.; Jiang, T.; Lin, J.; Gao, L.; Yang, C.; Wang, L.; Cai, C. Hierarchical Nanowires Synthesized by Supramolecular Stepwise Polymerization. *Angew. Chem., Int. Ed.* **2016**, *55*, 12522−12527.

(36) Yang, C.; Ma, X.; Lin, J.; Wang, L.; Lu, Y.; Zhang, L.; Cai, C.; Gao, L. Supramolecular "Step Polymerization" of Preassembled

DOI: 10.1021/jacs.9b07919
J. Am. Chem. Soc. 2019, 141, 16408−16415

Micelles: A Study of "Polymerization" Kinetics. *Macromol. Rapid Commun.* **2018**, *39*, 1700701.
(37) Ma, X.; Zhou, Y.; Zhang, L.; Lin, J.; Tian, X. Polymerization-Like Kinetics of the Self-Assembly of Colloidal Nanoparticles into Supracolloidal Polymers. *Nanoscale* **2018**, *10*, 16873−16880.
(38) Ma, X.; Gu, M.; Zhang, L.; Lin, J.; Tian, X. Sequence-Regulated SupracolloidalCopolymers via Copolymerization-LikeCoassembly of Binary Mixtures of PatchyNanoparticles. *ACS Nano* **2019**, *13*, 1968−1976.
(39) Li, T. I. N. G.; Sknepnek, R.; Macfarlane, R. J.; Mirkin, C. A.; Olverade la Cruz, M. Modeling the Crystallization of Spherical Nucleic Acid Nanoparticle Conjugates with Molecular Dynamics Simulations. *Nano Lett.* **2012**, *12*, 2509−2514.
(40) Li, T. I. N. G.; Sknepnek, R.; Olverade la Cruz, M. Thermally Active Hybridization Drives the Crystallization of DNA-Functionalized Nanoparticles. *J. Am. Chem. Soc.* **2013**, *135*, 8535−8541.
(41) Yu, Q.; Zhang, X.; Hu, Y.; Zhang, Z.; Wang, R. Dynamic Properties of DNA-Programmable Nanoparticle Crystallization. *ACS Nano* **2016**, *10*, 7485−7492.
(42) Yu, Q.; Hu, J.; Hu, Y.; Wang, R. Significance of DNA Bond Strength in Programmable Nanoparticle Thermodynamics and Dynamics. *Soft Matter* **2018**, *14*, 2665−2670.
(43) Zhu, G.; Xu, Z.; Yang, Y.; Dai, X.; Yan, L.-T. Hierarchical Crystals Formed from DNA-Functionalized Janus Nano-particles. *ACS Nano* **2018**, *12*, 9467−9475.
(44) Knorowski, C.; Burleigh, S.; Travesset, A. Dynamics and Statics of DNA-Programmable Nanoparticle Self-Assembly and Crystallization. *Phys. Rev. Lett.* **2011**, *106*, 215501.
(45) Knorowski, C.; Travesset, A. Dynamics of DNA-Programmable Nanoparticle Crystallization: Gelation, Nucleation and Topological Defects. *Soft Matter* **2012**, *8*, 12053−12059.
(46) Knorowski, C.; Travesset, A. Self-Assembly and Crystallization of Hairy (f-Star) and DNA-Grafted Nanocubes. *J. Am. Chem. Soc.* **2014**, *136*, 653−659.
(47) Glaser, J.; Nguyen, T. D.; Anderson, J. A.; Lui, P.; Spiga, F.; Millan, J. A.; Morse, D. C.; Glotzer, S. C. Strong Scaling of General-Purpose Molecular Dynamics Simulations on GPUs. *Comput. Phys. Commun.* **2015**, *192*, 97−107.
(48) Anderson, J. A.; Lorenz, C. D.; Travesset, A. General Purpose Molecular Dynamics Simulations Fully Implemented on Graphics Processing Units. *J. Comput. Phys.* **2008**, *227*, 5342−5359.
(49) Humphrey, W.; Dalke, A.; Schulten, K. VMD: Visual Molecular Dynamics. *J. Mol. Graphics* **1996**, *14*, 33−38.
(50) Odian, G. *Principles of Polymerization*; John Wiley & Sons: Hoboken, NJ, 2004.
(51) Gaynor, S. G.; Edelman, S.; Matyjaszewski, K. Synthesis of Branched and Hyperbranched Polystyrenes. *Macromolecules* **1996**, *29*, 1079−1081.
(52) Hadjichristidis, N.; Pitsikalis, M.; Pispas, S.; Iatrou, H. Polymers with Complex Architecture by Living Anionic Polymerization. *Chem. Rev.* **2001**, *101*, 3747−3792.
(53) Voit, B. I.; Lederer, A. Hyperbranched and Highly Branched Polymer Architectures Synthetic Strategies and Major Characterization Aspects. *Chem. Rev.* **2009**, *109*, 5924−5973.
(54) Fairbanks, B. D.; Scott, T. F.; Kloxin, C. J.; Anseth, K. S.; Bowman, C. N. Thiol-YnePhotopolymerizations: Novel Mechanism, Kinetics, and Step-Growth Formation of Highly Cross-Linked Networks. *Macromolecules* **2009**, *42*, 211−217.
(55) Wang, K. W.; Betancourt, T.; Hall, C. K. Computational Study of DNA-Cross-Linked Hydrogel Formation for Drug Delivery Applications. *Macromolecules* **2018**, *51*, 9758−9768.
(56) Hsu, C. W.; Sciortino, F.; Starr, F. W. Theoretical Description of a DNA-Linked Nanoparticle Self-Assembly. *Phys. Rev. Lett.* **2010**, *105*, 055502.
(57) Rovigatti, L.; Smallenburg, F.; Romano, F.; Sciortino, F. Gels of DNA Nanostars Never Crystallize. *ACS Nano* **2014**, *8*, 3567−3574.
(58) Starr, F. W.; Sciortino, F. Model for Assembly and Gelation of Four-Armed DNA Dendrimers. *J. Phys.: Condens. Matter* **2006**, *18*, L347−L353.
(59) Largo, J.; Starr, F. W.; Sciortino, F. Self-Assembling DNA Dendrimers: A Numerical Study. *Langmuir* **2007**, *23*, 5896−5905.
(60) Stockmayer, W. H. Molecular Distribution in Condensation Polymers. *J. Polym. Sci.* **1952**, *9*, 69−71.
(61) Xiong, H.; van der Lelie, D.; Gang, O. Phase Behavior of Nanoparticles Assembled by DNA Linkers. *Phys. Rev. Lett.* **2009**, *102*, 015504.
(62) Martinez-Veracoechea, F. J.; Mladek, B. M.; Tkachenko, A. V.; Frenkel, D. Design Rule for Colloidal Crystals of DNA-Functionalized Particles. *Phys. Rev. Lett.* **2011**, *107*, 045902.
(63) Rubinstein, M.; Colby, R. H. *Polymer Physics*; Oxford University Press: New York, 2003.

DOI: 10.1021/jacs.9b07919
J. Am. Chem. Soc. 2019, 141, 16408−16415